# Stereo Video Camera Calibration in the Wild

Arhum Sultana[a] and Michael Jenkin[b]
*Electrical Engineering and Computer Science, York University, Canada*
*{as14, jenkin}@ yorku.ca*

Keywords: Camera Calibration in the Wild, Stereo Video Processing.

Abstract: Although a number of robust stereo camera calibration algorithms exist in the literature, a common assumption of these algorithms is a representative set of calibration images containing a planar calibration target of known geometry. For stereo-video applications, it is a common practice to obtain a large number of stereo image pairs for the stereo calibration process. How should an optimal set of stereo-video calibration images be chosen when controlled camera positioning is difficult or impossible? Here we demonstrate how a greedy RANdom SAmple Consensus (RanSaC)-based approach can be used to choose the appropriate calibration image set for improved stereo camera calibration. This paper describes the performance of a greedy, RanSaC approach which is compared against a random frames selection approach. Performance is measured through mean calibration reprojection error. Evaluation on real world stereo video calibration data-sets collected in the underwater environment illustrates the effectiveness of the proposed approach.

## 1 INTRODUCTION

Fundamental to many computer vision algorithms is the need to calibrate the camera imaging system. Typically, the intrinsic and extrinsic parameters of the camera model are estimated numerically through the minimization of the reprojection error of a set of feature points extracted from a calibration target (Zhang et al., 1995; Torr and Zisserman, 2000; Hartley and Zisserman, 2003). A key concern for such optimization methods involves acquiring the 'right' calibration image set. A common approach is to take a few images of the calibration target, typically a 2D model plane with an easily imaged set of calibration points, under different orientations and positions by moving either the plane or the camera under ideal lighting conditions. This operational approach concisely encompasses two theoretical constraints: (i) Images should be taken of the calibration target over a range of different angles and external surface orientations – so as to capture the effects of the camera geometry on the imaging process; and equally critically that (ii) the number of images captured is reasonably small as the parameter estimation task includes a non-linear least-squares estimation process. This least-squares estimation process is sensitive to outliers in the calibration data-set and increasing the number of images increases the computational complexity of the task and the likelihood of including an outlier in the calibration set. When imaging a calibration target in the lab, there is typically a highly controlled process in direct control of the images that are captured and selected for camera calibration. But when the calibration data is collected out of doors (in the wild) with less positive control of the image capture process, it is a common practice to capture an extremely large number of images of the calibration target, and to deal with choosing the calibration set later. Deciding which of the collected image pairs to use for camera calibration is a challenging problem and choosing the wrong image set can have a significant impact on the calibration performance, and later stereo disparity matching and 3D reconstruction (Pollefeys et al., 2008; Engel et al., 2015; Poulin-Girard et al., 2016; Salvi et al., 2002). How can we choose the appropriate set of images from a video sequence to calibrate the camera? We consider this problem within the context of calibrating a stereo-video camera with a fixed base-line geometry separating the two cameras underwater.

Selecting the 'best' subset of these images by exhaustive search is unrealistic. For example if we wished to calibrate using a subset of 20 images, a typical number of calibration images for camera calibration, from a short video sequence(say 100 seconds with a camera capturing 30 frames a second), then there are $C_{20}(3000)$ or approximately $10^{51}$ possible

[a] https://orcid.org/0009-0004-1854-5444
[b] https://orcid.org/0000-0002-2969-0012

Sultana, A. and Jenkin, M.
Stereo Video Camera Calibration in the Wild.
DOI: 10.5220/0012191700003543
In *Proceedings of the 20th International Conference on Informatics in Control, Automation and Robotics (ICINCO 2023) - Volume 1*, pages 64-69
ISBN: 978-989-758-670-5; ISSN: 2184-2809

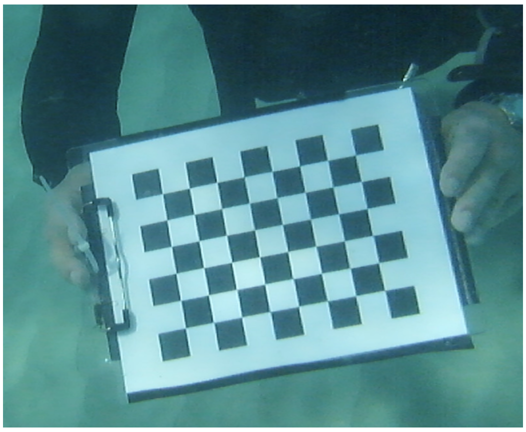

Figure 1: Sample target used for calibration. Here deployed underwater.

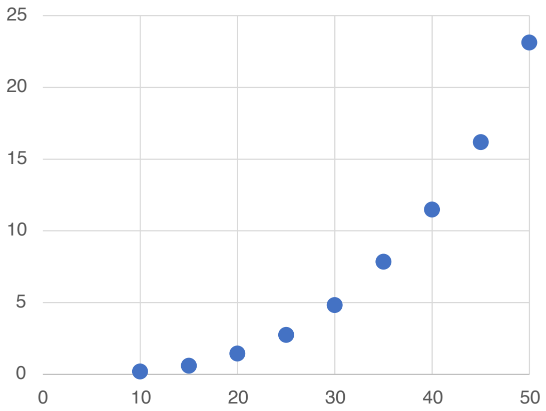

Figure 2: Computational cost of calibrating a monocular camera using the OpenCV camera calibration tool. Horiztonal axis is the number of camera frames in the calibration set. Vertical axis is the execution time in seconds. See text for details of the hardware/software environment.

sets to choose from. Clearly, a more structured approach is necessary to minimize this complex nature of the problem.

Here we explore the application of a simple RanSaC (Random Sample Consensus) (Fischler and Bolles, 1981) algorithm to recruit appropriate stereo image sets and compare this approach against repeated random sampling of the calibration image sets. We demonstrate that given a fixed computational budget RanSac provides an effective strategy for choosing the calibration frame set.

The remainder of this paper is organized as follows. Section 2 introduces the basic problem. Section 3 describes the simple RanSac approach used here. This approach is compared against multiple random calibrations of different calibration set sizes in Section 4. Finally, Section 5 summarizes the approach and suggests extensions to the work.

## 2 BACKGROUND

There exist a number of standard computer vision libraries, and OpenCV is representative. The OpenCV implementation of camera calibration is based on the Matlab calibration code and relies on Zhang's algorithm (Zhang, 2000) for calibration. Although a large number of options exist within both the OpenCV and Matlab libraries, the basic task for stereo camera calibration is typically structured as calibrating the two cameras separately and then solving for the camera separation geometry. Indeed, this is the basic approach suggested in the OpenCV documentation. Both the stereo camera separation and individual camera calibration processes are, in the Zhang algorithm-based codebase, based on a planar calibration target of $m$ calibration points (Figure 1) and the use of $n$ such targets. The monocular camera calibration process of Zhang's algorithm is based on minimizing the error between the projection of each of the $n \times m$ calibration points and their projection using the camera calibration, Specifically, to minimize

$$\sum_{I=1}^{n}\sum_{j=1}^{m} ||m_{i,j} - \hat{m}(A,R_i,t_i,M_j)||^2 \qquad (1)$$

where $m_{i,j}$ are the calibration points, $\hat{m}(A,R_i,t_i,M_j)$ is the estimation of the position of the calibration point resulting from the calibration process. $(R_i,\, t_i)$ defines the rotation and position of the $i$'th camera, and $M_j$ is the $j$'th calibration point. This is a non-linear optimization process that iterates its optimization until either a performance tolerance is obtained or a maximum number of interactions are performed. The critical observation here is that the number of iterations, and thus the computational cost/time, increases with the number of images in the calibration set.

To illustrate the effects of this, Figure 2 plots the computational cost of just the camera calibration stage (not including computing the location of the calibration corner points) for calibrating a monocular camera using OpenCV for calibration set sizes ranging from 10 to 50. Each calibration set was run ten times. Means and standard errors are plotted. The implementation was in Python3 running on a 16GB Apple M1 computer. Increasing set size results in a superlinear increase in computational cost.

Increasing the size of the calibration set does not necessarily improve calibration performance. This is illustrated in Figure 3 which shows mean and maximum error for randomly chosen calibration target sets. Each data point reflects ten calibration efforts of a given calibration set size. Although the mean cali-

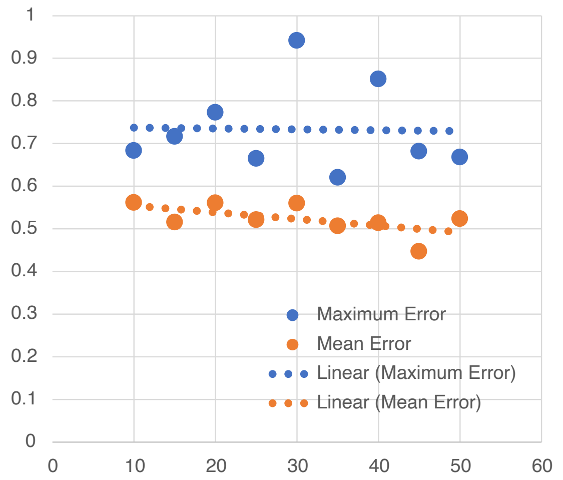

Figure 3: Mean and maximum RMS reprojection error for a monocular camera. Each data point corresponds to ten randomly chosen calibration target images. The horizontal axis shows the number of frames in the calibration set while the vertical axis is the re-projection error (in pixels). As the calibration set size increases the mean error decreases, although the maximum error does not.

bration error decreases with increasing calibration set size, the maximum error *increases* with increasing set size. This illustrates the sensitivity of the calibration process to outliers in the calibration frame set.

Selecting an appropriate calibration set in the wild is complicated by difficulties associated with selecting the appropriate set of frames and computational and calibration performance issues associated with just selecting a large set of frames for calibration.

## 3 SELECTING A STEREO CALIBRATION SET

The fundamental problem in calibrating a stereo video dataset in the wild is that the nature of the data collection process prevents the controlled selection of images of the calibration target. (This problem can also be found in monocular camera calibration, but here we concentrate on the stereo version of the problem.) We assume a set of $N$ stereo images of the calibration target and that for each of these $N$ stereo image pairs the target is properly captured in at least one of the left and right images of the target. We also assume that $N \gg 0$.

The basic problem in choosing a good set of image pairs is addressed using a greedy/RanSaC approach. The algorithm is applied to the left and right image sets to calibrate each camera separately. A final application of the algorithm is used to obtain the geometry between the two cameras. In each application of the algorithm, a small initial set of frames is selected, and additional stereo frames are added randomly to the set of frames as long as this reduces the RMS reprojection error of the set. This process is repeated a number of times and the best set of all of the frame sets identified is retained. The basic algorithm is sketched in Algorithm 1.

```
input  : S Initial set size, N maximum number
         of attempts to find a good calibration
         set, M maximum number of pairs to
         add to S, L maximum number of
         attempts to increase the set size before
         failure
output: bestModel the best set of calibration
         frames

bestModel ← None
i ← 0
while i < N do
    Initialize the calibration model by selecting
      S valid frames. This becomes the initial
      inlier set while the remaining frames
      becomes the initial outlier set.
    j ← 0
    success ← True
    while j < M and success do
        success ← False
        k ← 0
        while k < L and not success do
            Choose a random frame x from the
              outlier set. Compute MSE based
              on inlier ∪ {x}.
            if The MSE reduces relative to the
              MSE of the inlier set then
                Add x to the inlier set.
                Remove x from the outlier set
                Update the calibration model
                  with the new inlier set.
                success ← True
            end
            k ← k + 1
        end
    end
    if bestModel = None or model is better
      than bestModel then
        bestModel ← model
    end
end
```

Algorithm 1: Greedy/RanSaC stereo camera calibration. This process is run separately for the left and right image views using the valid set of left and right calibration images. The process is then repeated on the valid set of calibration images that provide both left and right views of the calibration target to obtain the geometry between the two cameras.

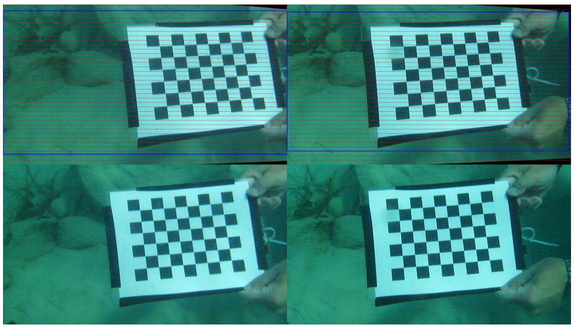

Figure 4: Sample calibration results from the RanSac-based frame selection algorithm. The bottom row shows one image pair from the input data stream, while the upper row shows that same pair after rectification following calibration. The rectified image shows the calibration region of interest (ROI) as well as overlaying horizontal lines showing that the calibration has resulted in corresponding features being aligned vertically.

In a traditional RanSaC algorithm the process of adding elements to the inlier set will also be accompanied by a process that removes outliers detected during the process from the inlier set. Here we avoid culling outliers from the set as we only add elements to the inlier set if they reduce the RMS error and we are particularly interested in having a range of different views in the calibration set.

In obtaining a valid set of stereo calibration frames we first process both the left and right images in each pair to obtain calibration points. Frames that do not obtain a valid left or right image of the calibration target are discarded. The set of valid left and valid right frames are used independently when selecting frames for the left and right cameras. This maximizes the set of possible frames for each camera. The set of frames with both left and right calibration images are used to calibrate the geometry between the cameras.

# 4 EVALUATION

In order to evaluate the stereo frame calibration algorithm we utilized a dataset of stereo video frames captured as part of a study of stereo video reconstruction of underwater structures. Data was collected using a Fuji W3 stereo camera in a custom underwater housing. Data was collected at 720p resolution. A standard OpenCV calibration target (see Figure 1) was used for calibration. As data was collected underwater at depth, accurate camera control was difficult. Surge moved both the camera operator and the target resulting in poor control of the camera during data collection.

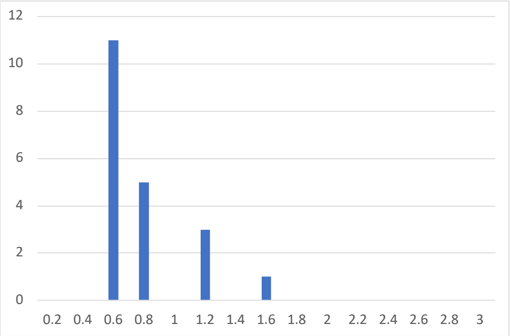

Figure 5: Histogram of stereo video calibration errors using Algorithm 1 from a single calibration sequence.

In order to explore the likely performance of Algorithm 1, the algorithm was used to calibrate the stereo camera with $N = 5$, $S = 15$, $M = 10$ and $L = 5$ using a single calibration dataset. Calibration was performed 20 times with a mean calibration time of approximately 240 seconds using the same hardware and software environment as described above. The mean calibration RMS error obtained with these parameters was 0.673 pixels. Results are plotted in Figure 5.

In order to evaluate the performance of Algorithm 1 against a random selection of stereo calibration frames, a version of the stereo video calibration framework was constructed that choose $n_l$ random image frames to calibrate the left camera, $n_r$ random frames to calibrate the right camera, and $s$ random stereo frames to calibrate the relationship between the two cameras. Average running time of this baseline with $n_l = n_r = s$ took approximately 1.5 seconds (for $s = 15$ frames), 7.12 seconds (for $s = 25$ frames) and 22 seconds (for $s = 35$ frames) to complete. Using the time taken for one run of Algorithm 1 with the parameters described earlier as a computational budget, one could perform almost 160 ($s = 15$), 34 ($s = 25$) or 11 ($s = 35$) efforts at calibrating the stereo camera pair using a random set of images using the same computational budget. Given a specific computational time budget, is it more effective to use the greedy RanSaC algorithm given in Algorithm 1 or to run calibration with random selections of frames of a given frame set size?

In order to explore this we used eleven different calibration sessions of the same underwater target shown in Figure 1 collected over a week off the western coast of Barbados. Calibration took place from 3m to 8m below the surface using the same Fuji W3 stereo camera as described earlier. Data was collected using a three-person diver team. One operating the camera, one operating the calibration target and one safety diver.

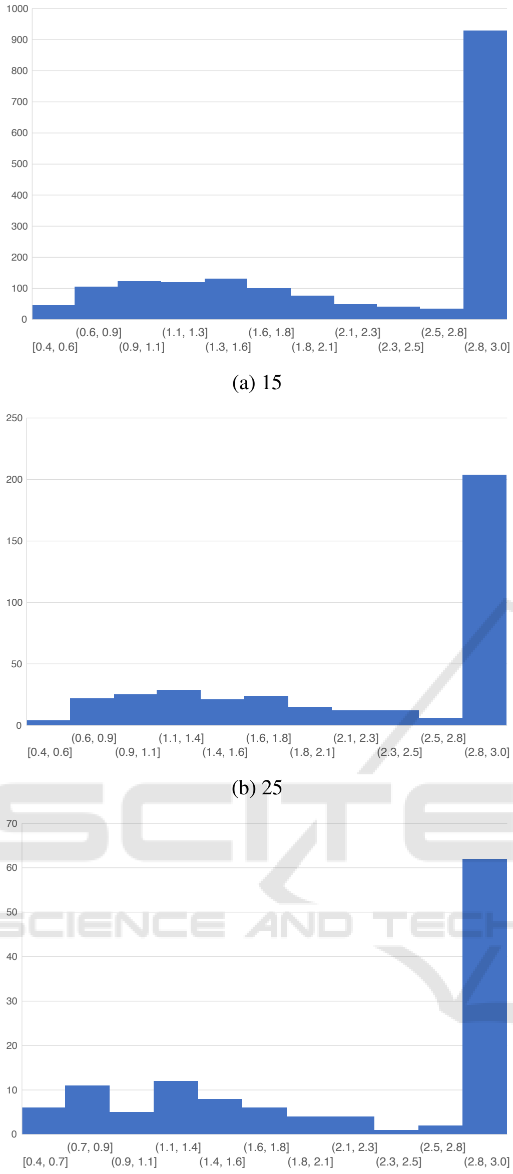

(a) 15

(b) 25

(c) 35

Figure 6: Histogram of stereo video calibration errors using the random frame strategy with different sized frame sets. Note that the right hand column in each graph includes all data points to the right of the distribution shown.

For each calibration set a single video recording was made, typically of 30-60 s in duration. For each of the eleven calibration sequences Algorithm 1 was run as were repeated calibration efforts using randomly chosen set sizes of 15, 25 and 35 frames. The set sizes were chosen to match the computational cost of Algorithm 1; 160 ($s = 15$), 34 ($s = 25$), and 11 ($s = 35$). Table 1 and Figure 6 summarize the performance of the RanSaC algorithm and the various random algorithms run with the same time budget. A random calibration approach was said to fail if it produced a RMS reprojection error of three pixels or more. This corresponds to the right most column in Figure 6.

Note that choosing a larger calibration set size does not necessarily result in an improvement in the resulting calibration. Choosing a RMS of three or higher as failure, then 43% of the random efforts result in failure with $s = 15$, 33% with $s = 25$ and 41% with $s = 35$. Although low RMS values are associated with smaller set sizes, such low sampling is unlikely to capture the full viewing space of the calibration target.

Although repeated random selection of calibration sets can produce a “good” calibration, and indeed outperform Algorithm 1, it also results in a number of calibrations that fail.

It is interesting to note that although the same camera calibration target, camera and underwater housing, and dive team were used for each of the data collection sessions there is a wide range of calibration performance results. Some data sessions (e.g., 1886) have relatively poor calibration performance across all of the algorithms tested, while in other sessions (e.g., 1895) each of the algorithms provided acceptable results, at least when choosing the ‘best’ error from the calibration set.

## 5 DISCUSSION

Calibrating a stereo camera rig in the wild introduces a range of issues that are not normally found under laboratory conditions. The underwater condition is perhaps the most challenging. Communication between individuals performing the calibration is difficult as is control of the calibration target and the imaging stereo rig. Nor is it straightforward to accurately monitor the camera capture process. Underwater camera viewfinders can be difficult to view when wearing SCUBA equipment, and it can be difficult or impossible to view both left and right camera views in real time. As a consequence, highly controlled imaging of the calibration target is not possible. Instead, a common approach is to collect a large amount of calibration data and then to choose which frames to process upon return to the lab. As ground truth of the calibration set – where the camera rig was relative to the calibration target – is not easily obtained, this selection process must operate in a poorly or uninformed manner. Here we have demonstrated that a greedy RanSac approach can produce calibration image sets that lead to good camera calibration. We also demonstrate that although the computational budget

Table 1: RanSac performance against random for multiple calibration datasets. ID is an identification number assigned to each set. Valid Frames refers to the number of frames in the dataset that gave rise to valid left (L), right (R) or stereo (S) images of the calibration target. RanSac RMS is the RMS projection error for one run of Algorithm 1, while Best, Mean and Fails are the best and mean RMS values for the Random Algorithm while Fails is the percentage of calibration efforts that resulted in a RMS error of three pixels or more. For some of the calibration sequences (e.g., 1886) random calibration sets perform poorly over all three set sizes. While for others (e.g., 1906) smaller set sizes performed quite well almost always.

| ID | Valid Frames | | | RanSac | Random 15 | | | Random 25 | | | Random 35 | | |
|---|---|---|---|---|---|---|---|---|---|---|---|---|---|
| | L | R | S | RMS | Best | Mean | Fails | Best | Mean | Fails | Best | Mean | Fails |
| 1886 | 689 | 680 | 680 | 8.48 | 1.14 | 35.3 | 96% | 1.52 | 39.2 | 97% | 2.14 | 31.5 | 90% |
| 1887 | 768 | 744 | 744 | 2.06 | 0.63 | 18.1 | 56% | 0.82 | 22.5 | 51% | 0.81 | 20.9 | 72% |
| 1895 | 687 | 694 | 687 | 0.48 | 0.47 | 9.40 | 43% | 0.73 | 12.8 | 48% | 0.51 | 4.47 | 9% |
| 1896 | 596 | 593 | 589 | 32.1 | 0.76 | 15.1 | 77% | 1.20 | 15.3 | 82% | 1.36 | 5.50 | 54% |
| 1905 | 932 | 929 | 929 | 2.25 | 1.13 | 30.8 | 87% | 1.36 | 40.3 | 94% | 20.8 | 43.6 | 100% |
| 1906 | 538 | 505 | 498 | 0.52 | 0.40 | 2.86 | 9% | 0.41 | 1.90 | 6% | 0.43 | 4.28 | 19% |
| 1915 | 636 | 636 | 636 | 5.40 | 0.74 | 13.7 | 89% | 1.09 | 11.7 | 67% | 1.46 | 21.3 | 81% |
| 1916 | 736 | 733 | 733 | 1.15 | 0.65 | 12.3 | 39% | 0.70 | 15.5 | 61% | 0.72 | 20.8 | 72% |
| 1923 | 402 | 401 | 401 | 1.98 | 0.82 | 2.29 | 16% | 0.88 | 1.87 | 9% | 1.01 | 1.86 | 18% |
| 1940 | 217 | 225 | 213 | 0.44 | 0.42 | 16.0 | 29% | 0.46 | 19.0 | 42% | 0.44 | 12.16 | 27% |
| 1941 | 469 | 497 | 468 | 1.08 | 0.84 | 4.92 | 19% | 0.96 | 6.86 | 27% | 1.13 | 3.23 | 9% |

to obtain these sets could be used to choose multiple sets of different sizes and then to just “take the best” resulting set, this approach is not guaranteed to produce a good set of views. Rather, many of these calibration efforts will produce camera calibrations that produce RMS errors much greater than three pixels. An error that will lead to stereo misalignment or significant error in recovered scene structure.

All that being said, in practice the calibration process in the lab has the advantage of providing for the calibration process to be run repeatedly until acceptable calibration performance results. We have found that a RanSaC greedy approach can be used to focus such repeated searches for a good calibration set in a way that does not require a predetermined calibration set size and which can use a greedy approach to select elements of the calibration set so as to optimize the RMS reprojection error.

The RanSaC algorithm (Algorithm 1) works to minimize the projection error. This is not the only error metric that might be used. For example, it would be possible to construct an error that not only sought to minimize the reprojection error but at the same time seeks to maximize the size of the calibration image set, or the distribution of camera poses used for calibration. This is the subject of ongoing investigation.

## ACKNOWLEDGEMENTS

The financial support of the NCRN and NSERC Canada is greatfully acknowledged.

## REFERENCES

Engel, J., Stückler, J., and Cremers, D. (2015). Large-scale direct SLAM with stereo cameras. In *IEEE/RSJ International Conference on Intelligent Robots and Systems (IROS)*, pages 1935–1942, Hamburg, Germany.

Fischler, M. A. and Bolles, R. C. (1981). Random sample consensus: A paradigm for model fitting with applications to image analysis and automated cartography. *Commun. ACM*, 24(6):381–395.

Hartley, R. and Zisserman, A. (2003). *Multiple View Geometry in Computer Vision*. Cambridge University Press.

Pollefeys, M., Nistér, D., Frahm, J.-M., Akbarzadeh, A., Mordohai, P., Clipp, B., Engels, C., Gallup, D., Kim, S.-J., Merrell, P., et al. (2008). Detailed real-time urban 3d reconstruction from video. *International Journal of Computer Vision*, 78(2-3):143–167.

Poulin-Girard, A.-S., Thibault, S., and Laurendeau, D. (2016). Influence of camera calibration conditions on the accuracy of 3d reconstruction. *Optics express*, 24(3):2678–2686.

Salvi, J., Armangué, X., and Batlle, J. (2002). A comparative review of camera calibrating methods with accuracy evaluation. *Pattern recognition*, 35(7):1617–1635.

Torr, P. H. and Zisserman, A. (2000). Mlesac: A new robust estimator with application to estimating image geometry. *Computer vision and image understanding*, 78(1):138–156.

Zhang, Z. (2000). A flexible new technique for camera calibration. *IEEE Transactions on Pattern Analysis and Machine Intelligence (PAMI)*, 22:1330–1334.

Zhang, Z., Deriche, R., Faugeras, O., and Luong, Q.-T. (1995). A robust technique for matching two uncalibrated images through the recovery of the unknown epipolar geometry. *Artificial intelligence*, 78(1-2):87–119.